Journal of Inflammation Research

Dovepress
Taylor & Francis Group

Open Access Full Text Article

ORIGINAL RESEARCH

An Integrated Machine Learning Framework for Developing and Validating a Diagnostic Model of Hub Genes Related to Lipid Metabolism in Chronic Rhinosinusitis

Panhui Xiong[1,*], Lei Liu[1,2,*], Jingting Pi[3,*], Ji Wang[1], Tao Lu[1], Xia Ke[1], Yu Jiang[1], Yang Shen[1], Yucheng Yang[1]

[1]Department of Otolaryngology Head and Neck Surgery, The First Affiliated Hospital of Chongqing Medical University, Chongqing, 400016, People's Republic of China; [2]Department of Otolaryngology Head and Neck Surgery, Mianyang Central Hospital, Mianyang, 621000, People's Republic of China; [3]Department of Otolaryngology Head and Neck Surgery, Yongchuan Hospital Affiliated of Chongqing Medical University, Chongqing, 402160, People's Republic of China

*These authors contributed equally to this work

Correspondence: Yucheng Yang; Yang Shen, Department of Otolaryngology Head and Neck Surgery, The First Affiliated Hospital of Chongqing Medical University, Chongqing, 400016, People's Republic of China, Email yychxh@163.com; sy_smile@sina.cn

Purpose: The study aimed to identify key genes related to lipid metabolism in chronic sinusitis and understand their biological implications, considering the growing interest in the association between chronic sinusitis - a complex inflammatory condition - and lipid metabolism due to lipids' role in inflammation and immunity.

Methods: Gene expression data from bulk - RNA sequence was analyzed and intersected with lipid metabolism genes and WGCNA module genes from the MSigDB database. Immune infiltration analysis was conducted. Machine learning techniques were used to develop a diagnostic model. qRT - PCR and immunofluorescence techniques were employed to confirm gene involvement. Potential targeted drugs were identified through relevant analyses.

Results: 41 hub genes were identified, which were involved in pathways like G protein - coupled receptor signaling, TGF - beta receptor signaling, and responses to oxidative stress and nitrogen compounds. Enrichment analyses suggested links to ubiquitin - mediated proteolysis, mTOR signaling, and MAPK signaling. A significant presence of immune cells was detected in the chronic sinusitis group. A combined RF+Stepglm model was developed, comprising six genes (KPNA3, RAB35, GLE1, RNF139, OSMR, and PDPK1), which demonstrated good diagnostic performance (AUC = 0.848). Potential targeted drugs such as Raloxifene and Hesperidin were identified. qRT - PCR and immunofluorescence confirmed that the expression levels of RAB35, GLE1, and OSMR were significantly higher in CRS samples compared to normal ones.

Conclusion: This research highlights the role of lipid metabolism in chronic sinusitis and provides a basis for the development of targeted therapies.

Keywords: chronic rhinosinusitis, lipid metabolism, hub gene, machine learning, diagnostic model, drug

Introduction

Chronic rhinosinusitis (CRS) is a persistent inflammatory disease affecting the sinonasal mucosa, with symptoms such as nasal obstruction, rhinorrhea, facial pain, and anosmia, impacting approximately 10% of the global population. CRS is typically categorized into two main types: CRS with nasal polyps (CRSwNP) and CRS without nasal polyps (CRSsNP), each with distinct pathophysiological features.[1] Despite extensive research, the precise pathophysiological mechanisms behind CRS remain unclear. Microbial dysbiosis, which has been demonstrated to play a role in CRS development in previous studies,[2] immune dysregulation supported by a wealth of research,[3,4] disruption of epithelial barrier function

Received: 25 April 2025
Accepted: 24 July 2025
Published: 30 July 2025

closely associated with CRS chronicity,[5] and neuroimmunity, a factor attracting increasing attention,[6] all contribute to its development and chronicity. Moreover, S. aureus can promote CRS through specific toxins or immune-mediated mechanisms.[7,8] Due to the persistence and protracted nature of chronic sinusitis, which seriously affects patients' quality of life, there is an urgent need for more effective diagnostic and therapeutic approaches.

Lipid metabolism, a critical regulator of inflammatory and immune pathways, has emerged as a significant factor in the pathogenesis of chronic rhinosinusitis (CRS). Numerous studies have highlighted the involvement of lipid mediators, such as leukotrienes and prostaglandins derived from arachidonic acid, in the development of CRS.[9] Additionally, concentrations of specialized pro-resolving mediators, particularly maresins, are reduced in the plasma of CRSwNP patients and are correlated with quality-of-life scores. MaR1, a key mediator, can regulate phagocyte activation, underscoring its crucial role in the pathophysiology of CRSwNP and its potential as a diagnostic marker.[10] Furthermore, dysregulated lipid mediator pathways have been linked to CRS endotypes, influencing microbiota composition and sustaining inflammation.[11] Adipocytokines, such as leptin and adiponectin, are not only involved in metabolic regulation but also play pivotal roles in immune responses. These factors, with pro-inflammatory (leptin) and anti-inflammatory (adiponectin) properties, can regulate mast cell functions and the synthesis of inflammatory mediators, thus influencing the course of immune inflammation.[12]

Existing diagnostic approaches for CRS often rely on subjective clinical assessments or imaging studies, which may not fully capture the underlying molecular drivers of the condition. Despite advances in genomics and metabolomics, there is a lack of robust diagnostic models that link lipid metabolism-related genes to CRS. Traditional statistical methods are difficult to effectively analyze. Machine learning algorithms such as random forests and support vector machines can automatically identify hidden patterns and feature associations in high-dimensional data, and capture key molecular features of disease occurrence and development through deep mining of patient omics data. Furthermore, no comprehensive frameworks exist to leverage machine learning for the identification and validation of hub genes associated with lipid metabolism in this context.

Previous studies have explored the relationship between CRS and gene sets such as mitochondria and neutrophil extracellular traps.[13,14] But to our knowledge, the relationship between lipid metabolism and CRS biomarkers has not been thoroughly explored. In order to fill these gaps, this study utilized our bulk-RNA sequence data and public resources, and applied advanced bioinformatics and machine learning methods to reveal key CRS biomarkers related to lipid metabolism, laying a theoretical foundation for CRS treatment strategies focusing on lipid metabolism.

Materials and Methods

Study Design and Participants

A flowchart of the study design is shown in Figure 1. This study included 22 patients who underwent surgery at the Department of Otolaryngology, First Affiliated Hospital of Chongqing Medical University from June 2022 to June 2023. The case group comprised 19 patients with CRS, while the control group consisted of 3 healthy individuals. The enrollment criteria are as follows: (1) Patients aged >18 years; (2) diagnosis of CRS based on EPOS2020 criteria;[15] (3) patients received ESS treatment during hospitalization; (4) Patients should stop taking oral corticosteroids 3 months before surgery, or stop intranasal steroid treatment 1 month before surgery. Additionally, patients who met the following criteria were excluded: (1) Patients with incomplete baseline blood routine, tissue specimen, sinus CT, and nasal endoscopy data; (2) aged < 18 years; (3) patients with granulomatous polyangiitis, eosinophilic granulomatous polyangiitis, sarcoidosis, cystic fibrosis, fungal rhinosinusitis, and sinus malignant tumor. The control group includes patients with deviated nasal septum who plan to undergo nasal septum plastic surgery. During the biopsy process, the middle turbinates were collected from these patients. The subjects in the control group did not experience upper respiratory tract infections or other types of sinusitis.

This study was approved by the Ethics Committee of the First Affiliated Hospital of Chongqing Medical University and conducted in accordance with the guidelines of the Helsinki Declaration of the World Medical Association (No.2022-K301) on June 17, 2022. Prior to the study, informed consent was obtained from all participants.

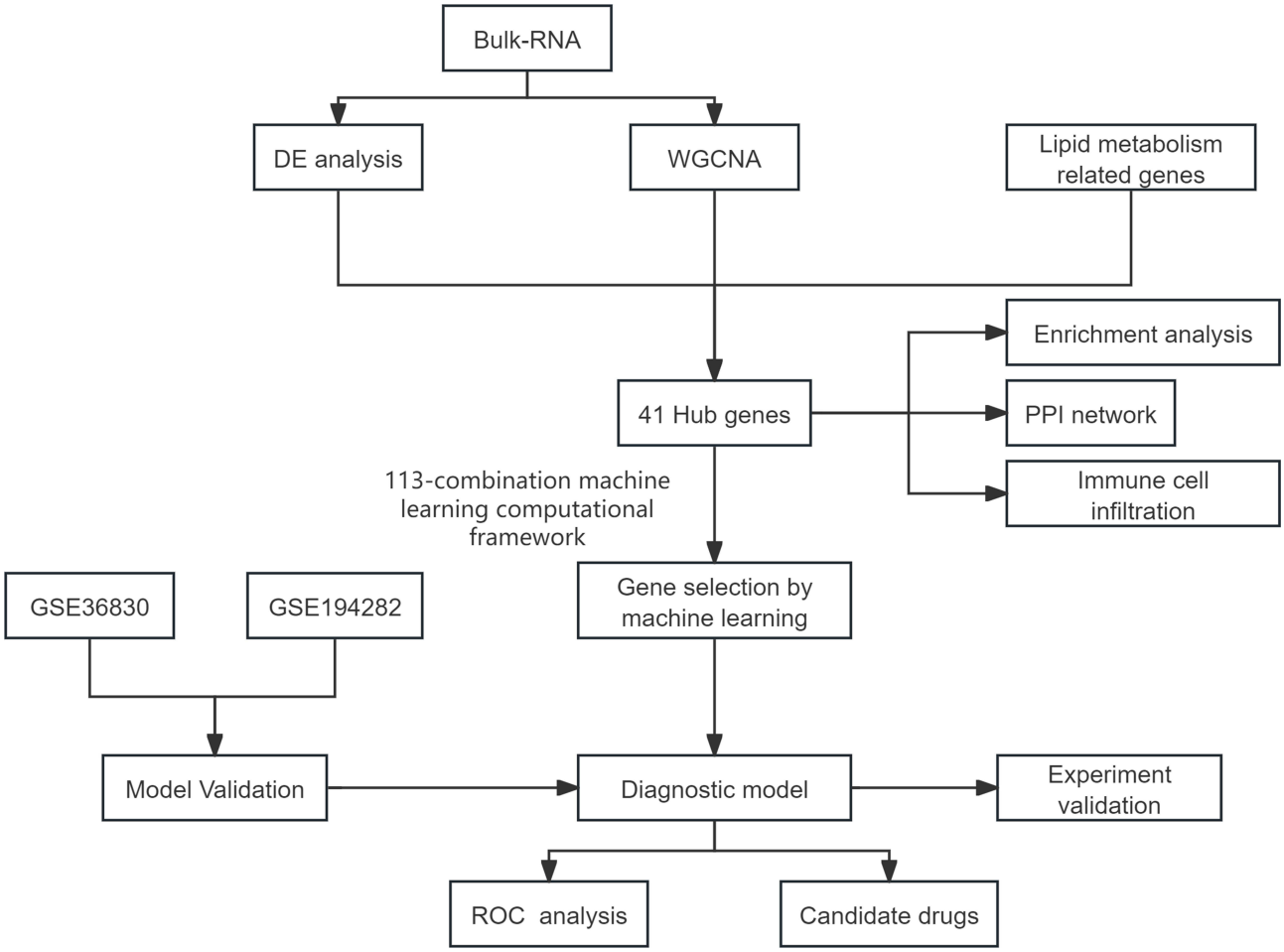

Figure 1 Flowchart of the analyses.

RNA-Seq Assay

Total RNA was extracted from a population of cells (1x106) via the protocol provided with TRIzol® reagent (Invitrogen, Shanghai, China). Library preparation and transcriptome sequencing were subsequently conducted at the Wuhan Genomics Institute (BGI, Wuhan, China) via MGISEQ-2000 technology, which resulted in the generation of 100 bp paired-end reads. The MGISEQ-2000 sequencing platform was used to quantify the read mapping counts for each gene. The number of fragments per kilobase of transcript per million fragments (FPKM) values were subsequently calculated for each gene. Fold change (FC) values were calculated to determine the differences in gene expression levels.

Data Collection

Partial gene expression data were retrieved from the NCBI Gene Expression Omnibus public database (GEO). The GSE194282 dataset comprises 7 CRS patients and 7 control patients. The GSE36830 dataset contains 18 CRS patients and 6 control patients. The specimens in these two datasets are either polyp or uncinate process tissues. These two datasets serve as external validation sets for machine learning models.

The lipid metabolic-related gene set was derived from the MEMBRANE gene set in the Molecular Signatures Database (http://www.gsea-msigdb.org/gsea/downloads.jsp). There are a total of 1995 genes within this gene set, and the specific details are presented in Supplementary Box 1.

Identification of Differential Expression Analysis

Differential expression analysis of CRS and Control samples was performed using the "limma" package in R software (version 4.4.1), with criteria of |log2 FC| > 0.25 and P-value <0.05. Heat maps and volcano plots of differentially expressed genes (DEGs) were generated using the "heatmap" and "ggplot2" packages.

Weighted Correlation Network Analysis (WGCNA)

Gene expression data from the samples were analyzed using the WGCNA package in R. First, a suitable soft-thresholding power was determined. We calculated the scale - free topology fit index for a series of soft-thresholding powers. The power value that led to a network with a scale - free topology index was selected. This ensured that the constructed network had the desired scale-free property.

Gene expression data from the samples were analyzed using the WGCNA package in R. First, a suitable soft-thresholding power was determined. We calculated the scale - free topology fit index for a series of soft-thresholding powers. The power value that led to a network with a scale - free topology index was selected. This ensured that the constructed network had the desired scale-free property.

After determining the soft-thresholding power, the adjacency matrix was computed based on the Pearson correlation coefficient of gene expression levels among genes. The formula for calculating the adjacency $\boldsymbol{\alpha ij}$ between gene $\boldsymbol{i}$ and gene $\boldsymbol{j}$ is $\boldsymbol{\alpha ij} = |\ \mathrm{cor}(\boldsymbol{xi}, \boldsymbol{xj})\ |^{\boldsymbol{\beta}}$, where $\boldsymbol{xi}$ and $\boldsymbol{xj}$ are the expression values of gene $\boldsymbol{i}$ and gene $\boldsymbol{j}$, respectively, and $\boldsymbol{\beta}$ is the soft - thresholding power. Subsequently, the topological overlap matrix (TOM) was derived from the adjacency matrix to better capture the complex relationships among genes.

Hierarchical clustering was then performed using the TOM - based dissimilarity measure. Modules were identified by applying the dynamic tree cut algorithm. Each module was assigned a unique color for identification purposes. The eigengene of each module, which represents the principal component of the gene expression within the module, was calculated. The correlations between module eigengenes and relevant clinical traits, such as disease severity, patient age, or treatment response, were analyzed to identify modules that were significantly associated with the traits of interest.

Identification of Hub Genes

To obtain the hub genes associated with lipid metabolism and CRS, we used the "VennDiaram" package in R software to identify the intersection among DEGs, the genes from WGCNA, and the lipid metabolic-related gene set. Box plots were used to show the differences in hub gene expression between CRS and control samples. Hypothesis testing was performed using the *t*-test and the Mann–Whitney *U*-test. The *t*-test was used for normally distributed data, and the Mann–Whitney *U*-test was used otherwise. Significance was defined as $P < 0.05$.

Protein-Protein Interaction Network

We retrieved protein-protein interaction (PPI) data from the Search Tool for the Retrieval of Interacting Genes/Proteins (STRING) database. We constructed the PPI network using the hub genes, with their interactions being represented as edges. By visualizing the network in Cytoscape (version 3.6.1), we analyzed the network's topology to identify hub genes.

Enrichment Analysis of Hub Genes

To explore the biological mechanisms by which hub genes affect CRS, enrichment analyses were performed. For the functional enrichment analysis of the gene set, we utilized the Gene Ontology (GO) annotations of genes within the R software package "org.Hs.eg.db" (version 3.1.0) as the background. During the Kyoto Encyclopedia of Genes and Genomes (KEGG) enrichment analysis, we utilized the KEGG REST API (https://www.kegg.jp/kegg/rest/keggapi.html) to acquire the most up-to-date gene annotations of the KEGG Pathway. The genes were then mapped onto this background set. Enrichment analysis was conducted using the R software package "clusterProfiler" (version 3.14.3) to obtain the gene set enrichment results. The minimum and maximum sizes of the gene set were set to 5 and 5000, respectively. Statistical significance was determined by a p-value less than 0.05 and a false discovery rate (FDR) less than 0.1.

Subsequently, for the Gene Set Enrichment Analysis (GSEA), the GSEA software (version 3.0) was acquired from the GSEA website (http://software.broadinstitute.org/gsea/index.jsp). Samples were divided into two groups based on median values of hub gene expression levels. The "c2.cp.kegg.v7.4.symbols.gmt" subset was downloaded from the Molecular Signatures Database to assess relevant pathways and molecular mechanisms. Considering the gene expression profiles and phenotype grouping, the minimum and maximum gene set sizes were set to 5 and 5000, respectively. With 1000 resamplings, statistical significance was considered when the P-value was less than 0.05 and the FDR was less than 0.25.

Immune Cell Infiltration

Single-sample gene set enrichment analysis (ssGSEA) was used to quantify the levels of 24 infiltrating immune cell types in each sample. These cell types are as follows: activated B cells, activated CD4 + T cells, activated CD8 + T cells, activated dendritic cells, CD56bright natural killer cells, CD56dim natural killer cells, eosinophils, basophils, gamma delta T cells, immature B cells, immature dendritic cells, MDSC, macrophages, mast cells, monocytes, natural killer T cells, natural killer cells, neutrophils, plasmacytoid dendritic cells, regulatory T cells, T follicular helper cells, Type 1 T helper cells, Type 17 T helper cells, and Type 2 T helper cells.

Machine Learning Algorithms

In this study, we perform an in - depth analysis of the data with machine-learning algorithms. Firstly, the raw data undergoes pre - processing, which involves removing missing values and outliers. Z - score standardization is then applied to make the mean of each feature 0 and the standard deviation 1, thereby eliminating the influence of different feature scales. To address batch effects in the data, this study used the ComBat algorithm to adjust the covariates of different batches of data, making the data distribution more consistent and reducing error interference caused by batch differences. Subsequently, The bulk-RNA sequence is used as the training set, while the GSE194282 dataset and the GSE36830 dataset are used as the test set. During the model-training phase, we employ multiple machine-learning algorithms to assess their performance, namely Elastic Net regression ($\lambda = 0.1$), Lasso regression ($\lambda = 0.05$), Ridge regression ($\lambda = 1.0$), Support Vector Machine (SVM, $C = 1.0$, $\gamma = 0.01$), Linear Discriminant Analysis (LDA), Gradient Boosting Machine (GBM, with a learning rate of 0.1 and 100 trees), Random Forest (RF, with 200 trees), and XGBoost (XGB, with a learning rate of 0.01 and 150 trees). These models are trained on the training set, and the hyperparameters are optimized through cross - validation. In the model - evaluation stage, the Area Under the Curve (AUC) value of each model (with a threshold of 0.7) is calculated using the test set to gauge its classification performance. Finally, the AUC values of all models are computed by the RunEval function, and a heat map is generated by the SimpleHeatmap function for visualizing the performance of each model. The model with the highest AUC value is chosen as the final optimal model.

Identification of Drug Candidates

Based on hub genes and their associated pathways, we searched the Drug Signature Database (DSigDB) in the Enrichr web platform (https://amp.pharm.mssm.edu/enrichr/) for potential drug candidates.

RNA Extraction and Quantitative Real-Time Polymerase Chain Reaction (qRT-PCR)

The extraction of total RNA was carried out as previously described. The quality of the extracted RNA was verified using spectrophotometers. Subsequently, approximately 200 ng of the total RNA was reverse-transcribed into complementary DNA (cDNA) using the ABScript Neo RT Master Mix (RK-20433,ABdonal, Wuhan, China).To quantify the RNA expression level, qRT-PCR was employed. The cDNA was amplified using the SYBR Green PCR Master Mix (HY-K0523, MCE, Monmouth Junction, NJ, USA). Relative gene expression analysis was performed on the CFX Connect Real -Time PCR Detection System (Bio - Rad, Hercules, CA, USA). The 2-ΔΔCT method was utilized for data analysis, with β-actin serving as the internal control. The primer sequences used in qRT-PCR are shown in Supplementary Table 1.

Immunofluorescence

Paraffin-embedded NP and normal samples were first deparaffinized with xylene and then underwent progressive dehydration in a series of ethanol solutions: 100%, 95%, 85%, and 70% ethanol, each for 5 minutes. Subsequently,

the sections were incubated overnight at 4°C with the following primary antibodies: rabbit-anti-RAB35 (diluted 1:150,11,329-2-AP, Proteintech, China), rabbit-anti -GLE1 (diluted 1:200, 26,466-1-AP, Proteintech, China), and rabbit-anti-10982-1-AP (diluted 1:100, 10,982-1-AP, Proteintech, China).After being washed with PBS, the sections were treated with secondary antibodies (SA00013-4, Proteintech, corallite488 - conjugated Goat, China) for 30 minutes. Then, the nuclei were labeled by staining with DAPI (Abcam, USA) at room temperature in the dark. Finally, the stained sections were visualized using a fully automated section scanning system (SP8, Leica, Germany).

Statistical Analysis

In this investigation, we utilized R software (version 4.4.1) for statistical computations and visualization of bioinformatics datasets. Additionally, GraphPad Prism (San Diego, CA, USA) and SPSS (IBM SPSS, Chicago, IL, USA) were used to analyze our experimental data delineated as mean ± standard deviation (SD). Binary comparisons were addressed using the *t*-test, while multiple group assessments using one-way ANOVA. A threshold of $P < 0.05$ was established for statistical significance.

Results

This study screened 4768 differentially expressed genes (DEGs) from CRS patients and control groups, and further identified six key genes closely related to CRS lipid metabolism, including KPNA3, RAB35, GLE1, RNF139, OSMR, and PDPK1. Functional enrichment analysis showed that ubiquitin mediated protein hydrolysis mTOR Neurotrophic factors and MAPK signaling pathways are closely related to inflammation and immune regulation. Immune cell infiltration analysis showed significant differences in the expression of various immune cells such as activated B cells and CD8+T cells in CRS patients. In addition, the RF+Stepglm [both] model constructed in the study showed excellent diagnostic performance (AUC=0.848), and potential drugs targeting related genes were proposed. qRT-PCR and immunofluorescence experiments confirmed that RAB35, GLE1, and OSMR genes positively correlated with CRS in the model were significantly upregulated in CRS patients.

Identification of Differentially Expressed Genes Associated with CRS

To identify the differential genes between CRS and the control group, we initially obtained 4768 differentially expressed genes (see Supplementary Table 2) from our bulk-RNA sequence under the screening criteria of "|log2 FC| > 0.25 and P_value <0.05". Subsequently, we generated the heatmap of the top 50 differentially expressed genes (Figure 2A) and the scatter plot of these differentially expressed genes (Figure 2B).

Identification of Hub Genes Associated with Lipid Metabolism-Related CRS

We utilized the gene expression profiles to calculate the Median Absolute Deviation (MAD) for each gene respectively. By removing the top 50% of genes with the smallest MAD values, the expression profiles of 9,463 genes and 22 samples can be extracted from the bulk-RNA sequence for constructing a weighted gene co - expression network. When the soft - thresholding power is set to 9, the scale - free topology fit index reaches 0.85 and the mean connectivity is 109.51 (Figure 3A and B). When the minimum module size was set to 30, the cut height to 0.25, the sensitivity to 3, and the module merging threshold to 0.25, 23 distinct co - expression modules were obtained through dynamic tree cutting (Figure 3C). Subsequently, a correlation analysis was conducted between each module and the clinical features (Figure 3D and E). The MEcoral1 module exhibited the highest positive correlation with the CRS group ($r = 0.73$, $p = 1.2\times e\text{-}4$), while the MEpurple module presented the highest negative correlation with CRS ($r = -0.91$, $p = 5.8\times e\text{-}9$). Based on the gene quantity and correlation, we selected the MEantiquewhite4 module which encompasses 475 genes (see Supplementary Table 3). At this point, the correlation analysis between MM and GS reveals that these genes are highly correlated with both the module and the phenotype ($r = 0.34$, $p = 3.5e - 94$, Figure 3F). Forty-one hub genes, including MET, BFAR, RAB35, GCNT1, PEX13, OSMR, CDC42, CLNS1A, NUP50, TM9SF2, BCL2L13, ATP6V1A, ATP2B4, SYK, GLE1, CEPT1, CDC42SE1, DNM2, CTNNB1, SSH1, KPNB1, ARCN1, RNF139, PARP1, PNPLA8, STT3B, LEMD3, CSNK2A1, KPNA3, NDUFS1, MAN1A2, NCSTN, LMAN1, IL6R, NUP98, KPNA1, ATP2A2, PDPK1, CDC42BPB, COPA and XPO7, associated with lipid metabolism and CRS were obtained by us from 4768 differentially - expressed genes (DEGs), 475 MEantiquewhite4 module genes and 1995 lipid metabolic - related genes within our bulk-RNA sequence (Figure 4A). Box plots were utilized to present the expression of each gene in the CRS group and the control

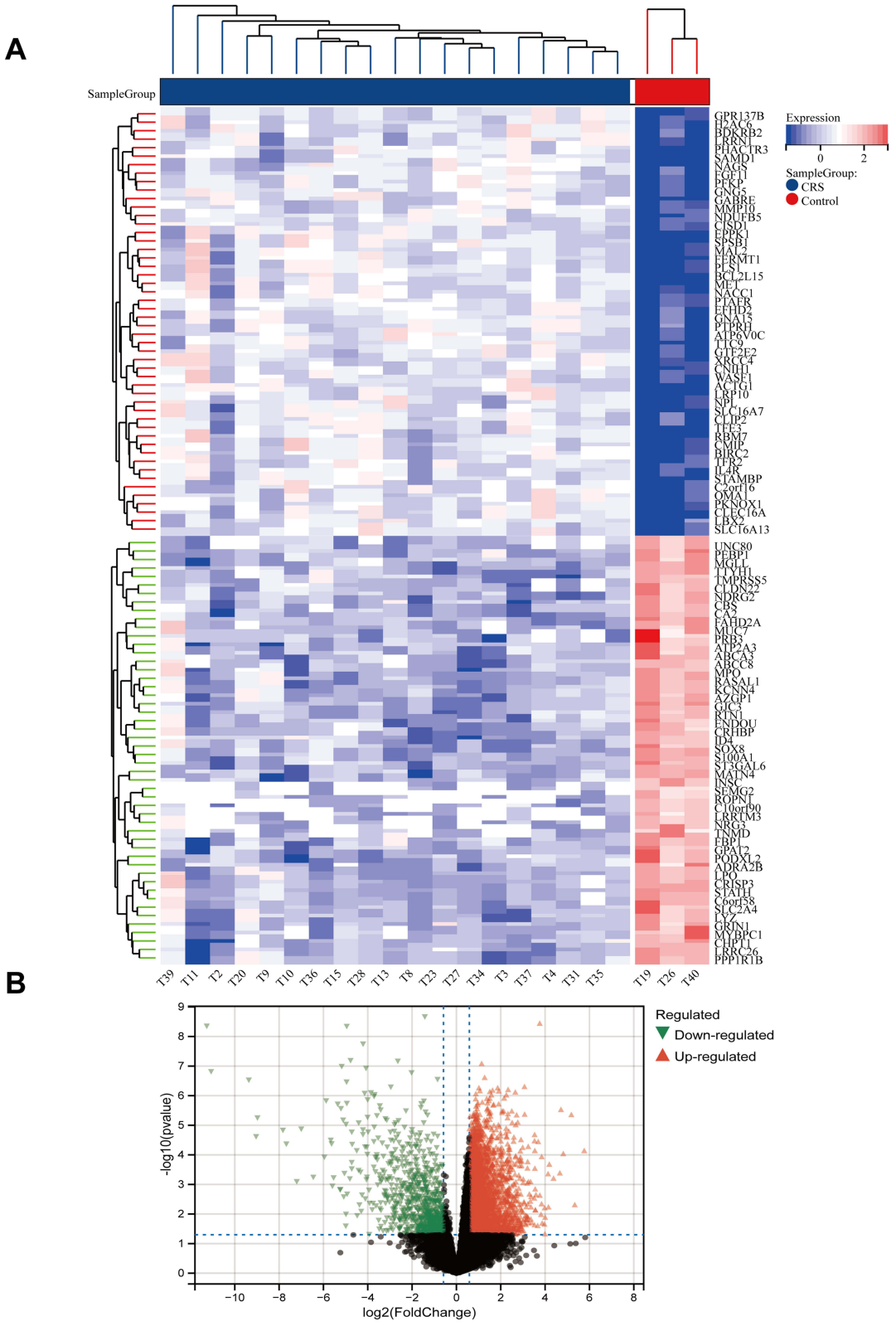

Figure 2 Differentially expressed genes between the CRS group and the normal group. (**A**) Heatmap showing the top 50 genes significantly highly expressed in the CRS or normal group. (**B**) Red genes represent significantly high expression in CRS, green genes represent significantly low expression in CRS, and gray genes indicate nonsignificant changes.

https://doi.org/10.2147/JIR.S536790

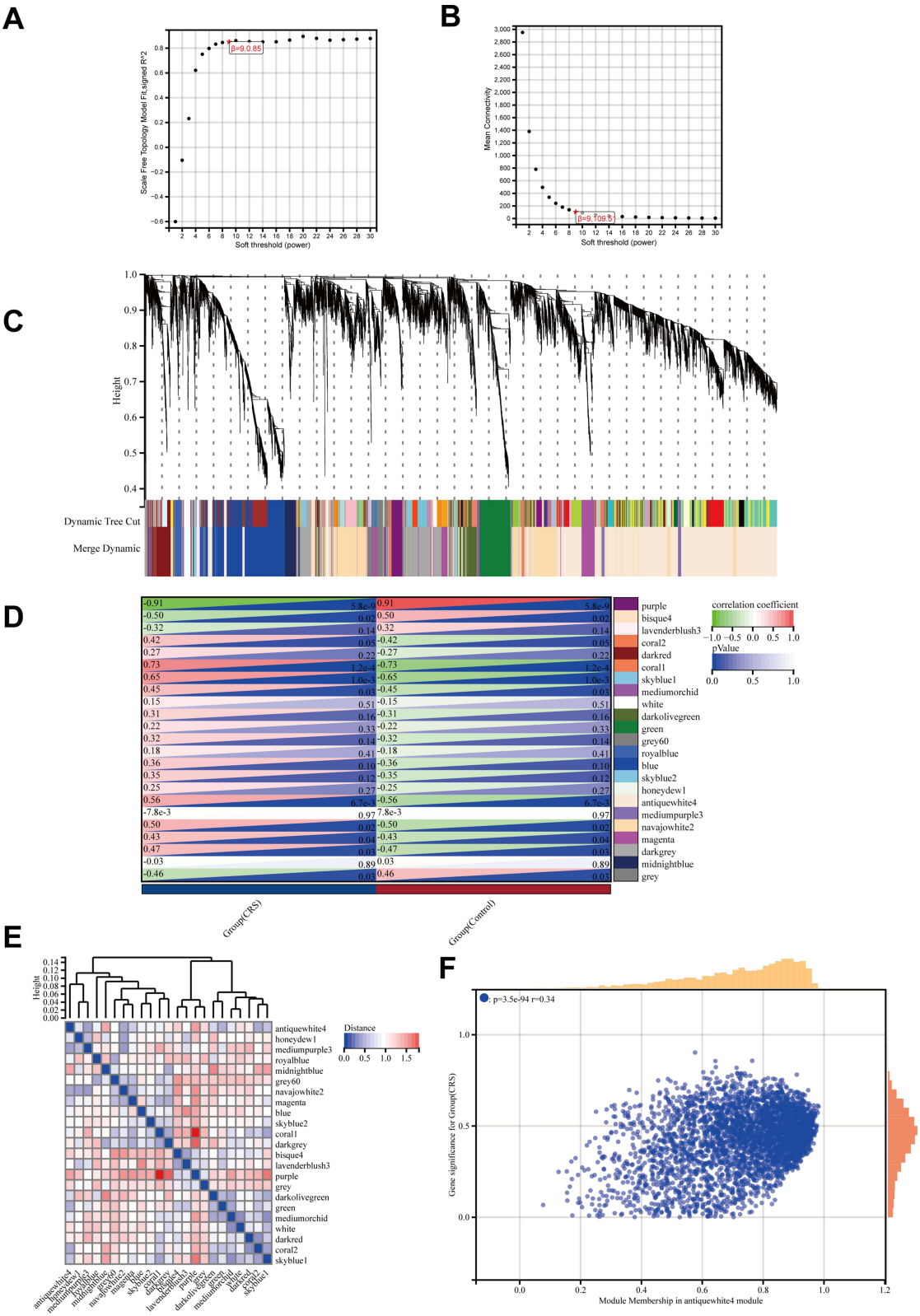

Figure 3 Results of the WGCNA. (**A**) The corresponding scale–free topological model fit indices at different soft threshold powers. (**B**) The corresponding mean connectivity values at different soft threshold powers. (**C**) Cluster dendrogram of genes. (**D**) Correlations between different modules and clinical traits. (**E**) Module eigenvector clustering. (**F**) Correlation between module membership and gene significance in the antiquewhite4 module. The red star symbol: the best soft threshold parameter.

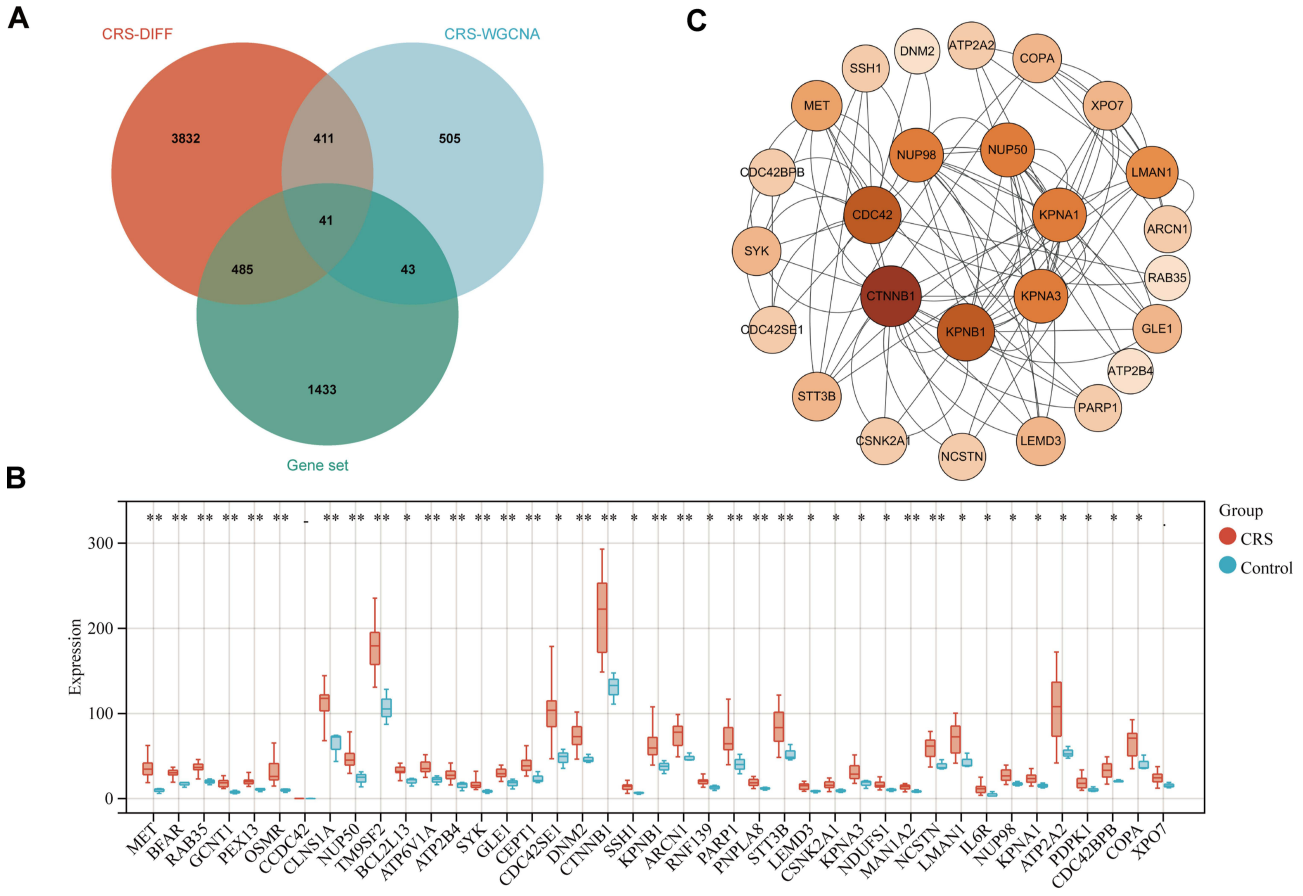

Figure 4 Hub genes and PPI network analysis. (**A**) Forty-one hub genes were obtained by taking the intersections of the DEGs, MERantiquewhite4 module genes of the WGCNA, and lipid metabolism–related genes. (**B**) PPI network of the 41 common genes constructed via GeneMANIA. (**C**) Violin plots of the expression of hub genes in the CRS group and the control group. *P < 0.05; **P < 0.01; -, not significant; •, marginally significant, 0.05 < P < 0.10.

group respectively (Figure 4B). It was found that the expression levels of the majority of hub genes in the CRS group were higher than those in the control group, and the difference was statistically significant.

Functional Enrichment of Hub Genes Involved in Lipid Metabolism -Related CRS

The PPI (Protein - Protein Interaction) network of the hub gene set and its closely associated genes was established by using STRING and Cytoscape (Figure 4C). Furthermore, enrichment analysis of the pathways related to the hub genes was carried out via the Reactome database (https://reactome.org/). The potential pathways are as follows: NS1 Mediated Effects on Host Pathways, Transport of Ribonucleoproteins into the Host Nucleus, ISG15 antiviral mechanism, Influenza Infection, Inhibition of nitric oxide production, Infectious disease, Vpr-mediated nuclear import of PICs, Nuclear import of Rev protein, GPVI-mediated activation cascade and Apoptotic execution phase (Figure 5A). GO enrichment analysis revealed overrepresentation of biological processes including negative regulation of G protein-coupled receptor signaling pathway, transforming growth factor beta receptor signaling pathway, cellular response to oxidative stress, T cell activation, glycoprotein metabolic process, enzyme linked receptor protein signaling pathway, response to nitrogen compound, and protein modification process (Figure 5B). Enriched cellular components included nuclear pore, host, host cell, nuclear envelope, membrane protein complex, organelle subcompartment, organelle membrane, and endomembrane system (Figure 5C). Overrepresented molecular functions comprised calcium-transporting ATPase activity, nitric-oxide synthase binding, nuclear import signal receptor activity, protein kinase binding, purine ribonucleoside triphosphate binding, nucleotide binding, nucleoside phosphate binding and enzyme binding (Figure 5D). From the perspective of comprehensive GO analysis, those key terms in the top positions are shown in the circle plot (Figure 5E) according to the ranking order of the P_adjust-value from low to high. The KEGG enrichment analysis of hub genes included PI3K-Akt

https://doi.org/10.2147/JIR.S536790

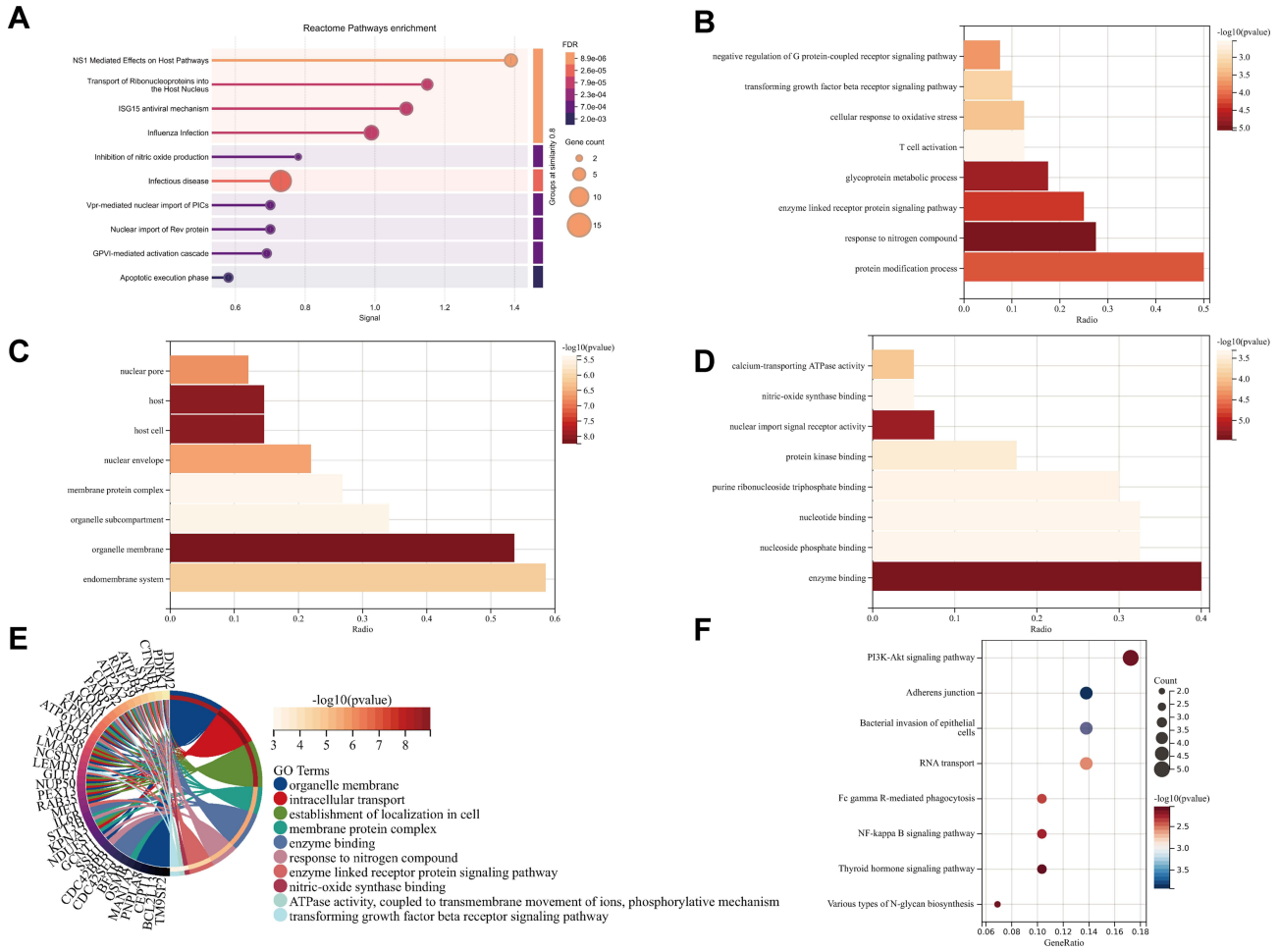

Figure 5 Enrichment analyses. (**A**) Reactome pathways enrichment. (**B**) Bar plots of GO enrichment analysis results for biological processes. (**C**) Bar plots of GO enrichment analysis results for cellular components. (**D**) Bar plots of GO enrichment analysis results for molecular function. (**E**) Circle plot of GO enrichment analysis results. (**F**) Bubble plot of KEGG enrichment analysis results.

signaling pathway and Adherens junction, Bacterial invasion of epithelial cells, NF-kappa B signaling pathway and Various types of N-glycan biosynthesis (Figure 5F).

Immune Cell Infiltration Analysis of Hub Genes Involved in Lipid Metabolism-Related CRS

Immune infiltration can reveal the role of the immune microenvironment in the occurrence and development of diseases. We initiated a comprehensive and profound analysis of immune cell infiltration on our bulk-RNA sequence dataset. During this analytical process, particular attention was paid to the expression levels of diverse immune cell types in both the CRS group and the control group. Notably, sixteen immune cell types—activated B cells, activated CD8 + T cells, activated dendritic cells, gamma delta T cells, immature B cells, MDSC, macrophages, mast cells, monocytes, natural killer cells, neutrophils, plasmacytoid dendritic cells, regulatory T cells, T follicular helper cells, Type 1 T helper cells, basophils and Type 2 T helper cells—showed remarkably significant differences in expression between the CRS and control groups (Figure 6).

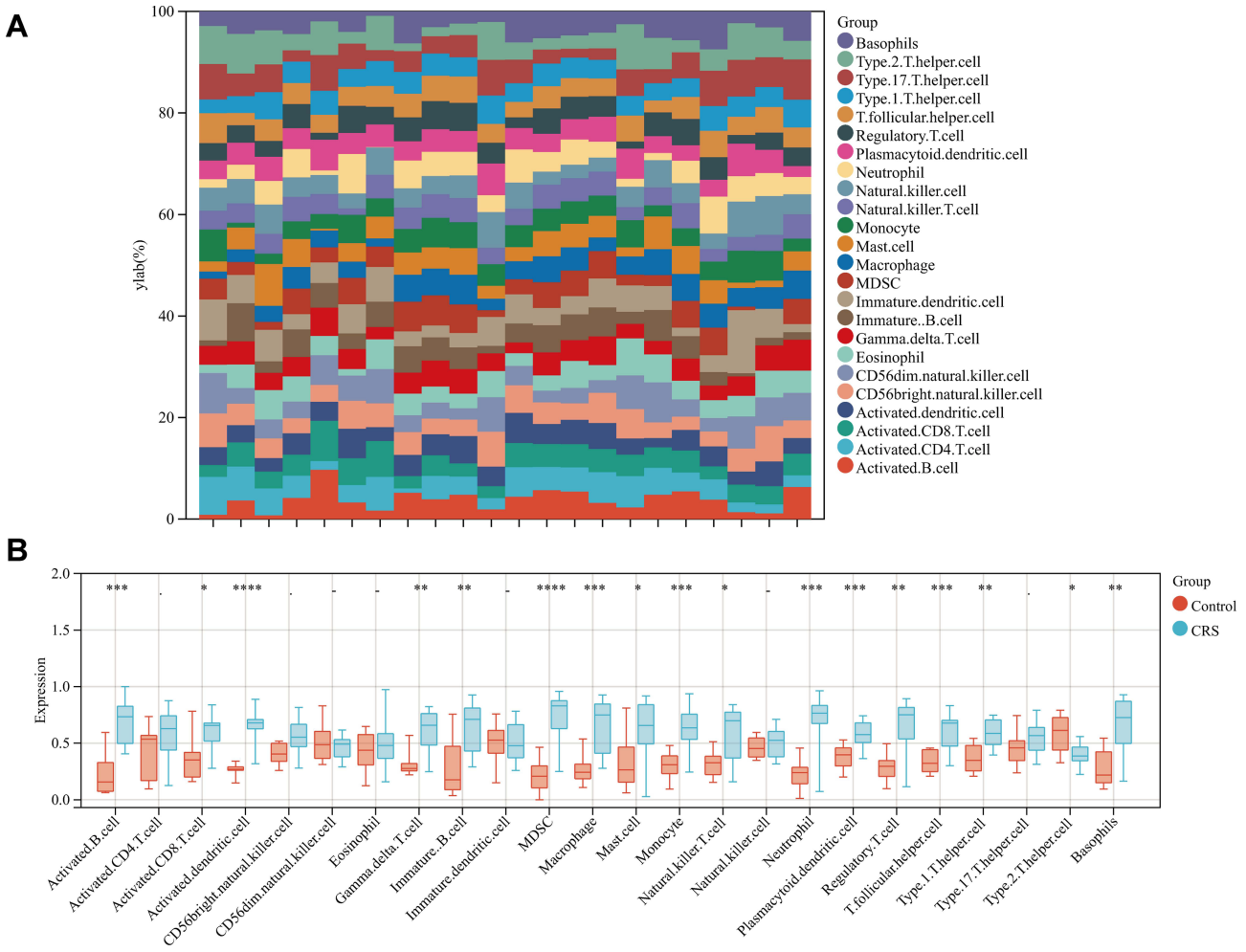

Figure 6 Immune infiltration in CRS and control samples. (**A**) The relative percentage of 23 immune cells in each sample. (**B**) Differences in immune infiltration between CRS and control samples. *P < 0.05; **P < 0.01; ***P < 0.001; ****P < 0.0001; -, not significant; •, marginally significant, 0.05 < P < 0.10.

Construction a Diagnostic Model for Lipid Metabolic-Related CRS via Machine Learning

In the process of 10-fold cross-validation of 12 machine-learning algorithms, they were combined to identify the most accurate diagnostic model based on 41 hub genes (Figure 7A). This analysis was carried out in the training dataset (bulk-RNA sequence) as well as two external validation datasets (GSE36830 and GSE194282). The selected optimal diagnostic model turned out to be the RF+Stepglm[both], which identified all 6 key genes: KPNA3, RAB35, GLE1, RNF139, OSMR, PDPK1. This prediction model exhibits excellent diagnostic performance, with an AUC value of 0.895 (Figure 7B). Then, we further verified this model. The AUC values of the model in GSE194282 and GSE36830 were relatively high, specifically 0.898 and 0.750 respectively (Figure 7C and D). The calibration curve of our diagnostic model (Figure 7E) closely approximates the ideal diagonal in both cohorts. This implies an optimal degree of consistency between the predicted probabilities obtained from the model and the actual clinical outcomes that have been observed, thus manifesting robust calibration performance.In the decision curve analysis (Figure 7F), the net benefits of all models were better within the threshold probability range. Figure 7G presents the Nomogram of these 6 key genes. GSEA of these genes has shown that they are associated with ubiquitin-mediated proteolysis, the mTOR signaling pathway, neurotrophin signaling, and MAPK signaling (Figure 8).

https://doi.org/10.2147/JIR.S536790

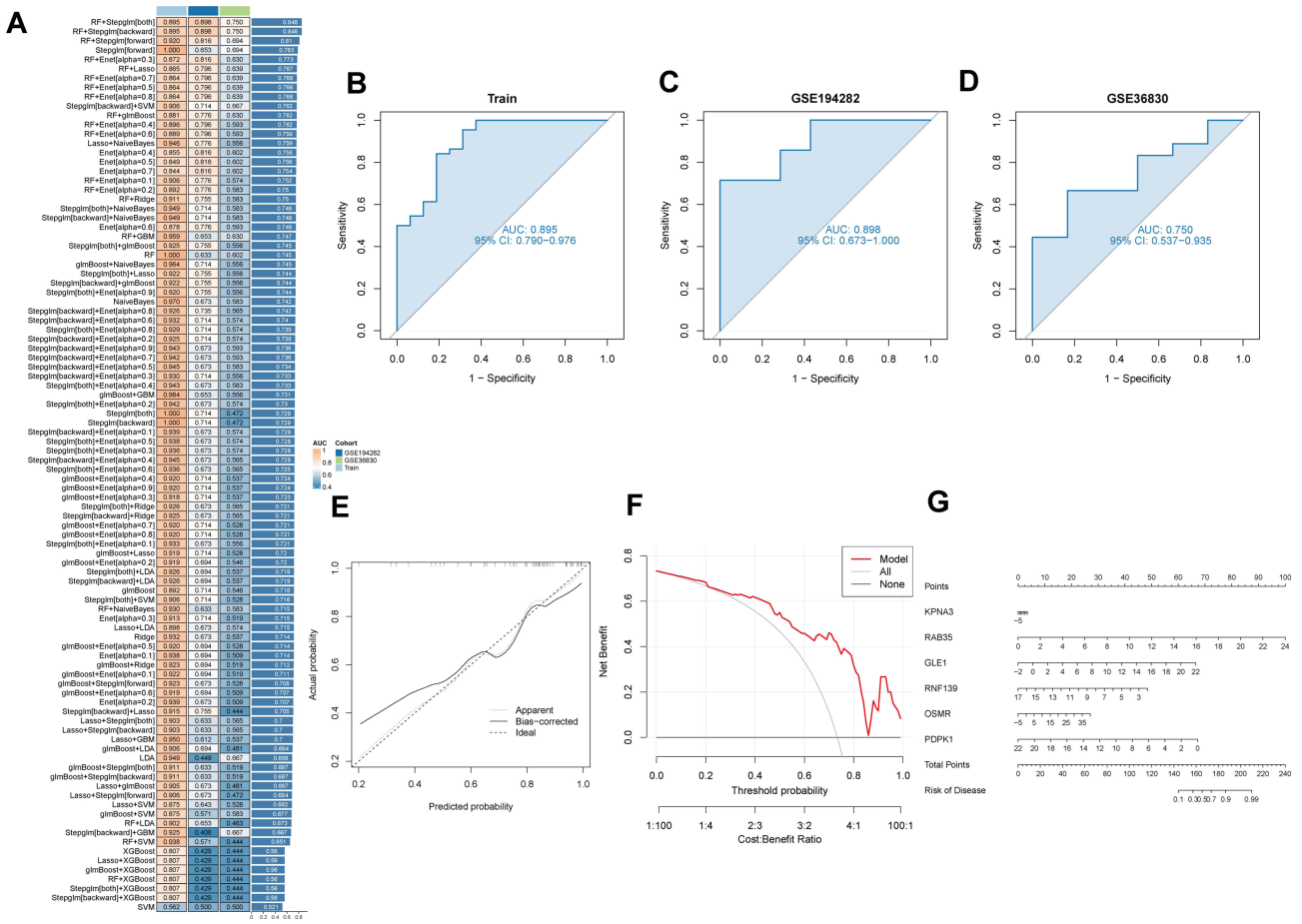

Figure 7 Diagnostic performance of our model. (**A**) 113 machine learning algorithm combinations evaluated via 10–fold cross–validation. (**B**) ROC curves of the training cohort. (**C** and **D**) ROC curves of the testing cohort. (**E**) Calibration curve of the training cohort. (**F**)The decision curve analysis of the training cohort. (**G**) Nomogram.

Identification of Candidate Drugs

The model genes were analyzed using the DSigDB drug database on Enrichr to identify potential targeting agents. Some of the candidate drugs with statistical differences are Raloxifene, Hesperidin, fulvestrant MCF7 DOWN, estradiol CTD 00005920, oxindole i TTD 00009978, LY-294002 HL60 UP, 0175029–0000 MCF7 DOWN, bisindolylmaleimide i TTD 00002466, 0316684–0000 MCF7 DOWN, paclitaxel CTD 00007144 (Table 1). The remaining relevant candidate drugs are presented in Supplementary Table 4.

Experimental Validation

The expression levels of the genes RAB35, GLE1, and OSMR, which were positively correlated with CRS in the model, were validated through qRT-qPCR. The results for these genes in CRS and normal samples suggest that the mRNA expression levels of these genes were significantly higher in CRS samples compared to normal samples ($P < 0.05$), as shown in Figure 9A.Furthermore, immunofluorescence was employed to detect the protein expression levels of these three genes. The immunostaining intensities of RAB35, GLE1, and OSMR were stronger in CRS samples compared to those in normal samples (Figure 9B–G).

Discussion

This study applied advanced bioinformatics and machine learning to investigate the relationship between lipid metabolism and CRS. Key findings include the identification of 4,768 DEGs from patients with chronic sinusitis and the control group, narrowed down to six key genes—KPNA3, RAB35, GLE1, RNF139, OSMR, and PDPK1—which play a pivotal

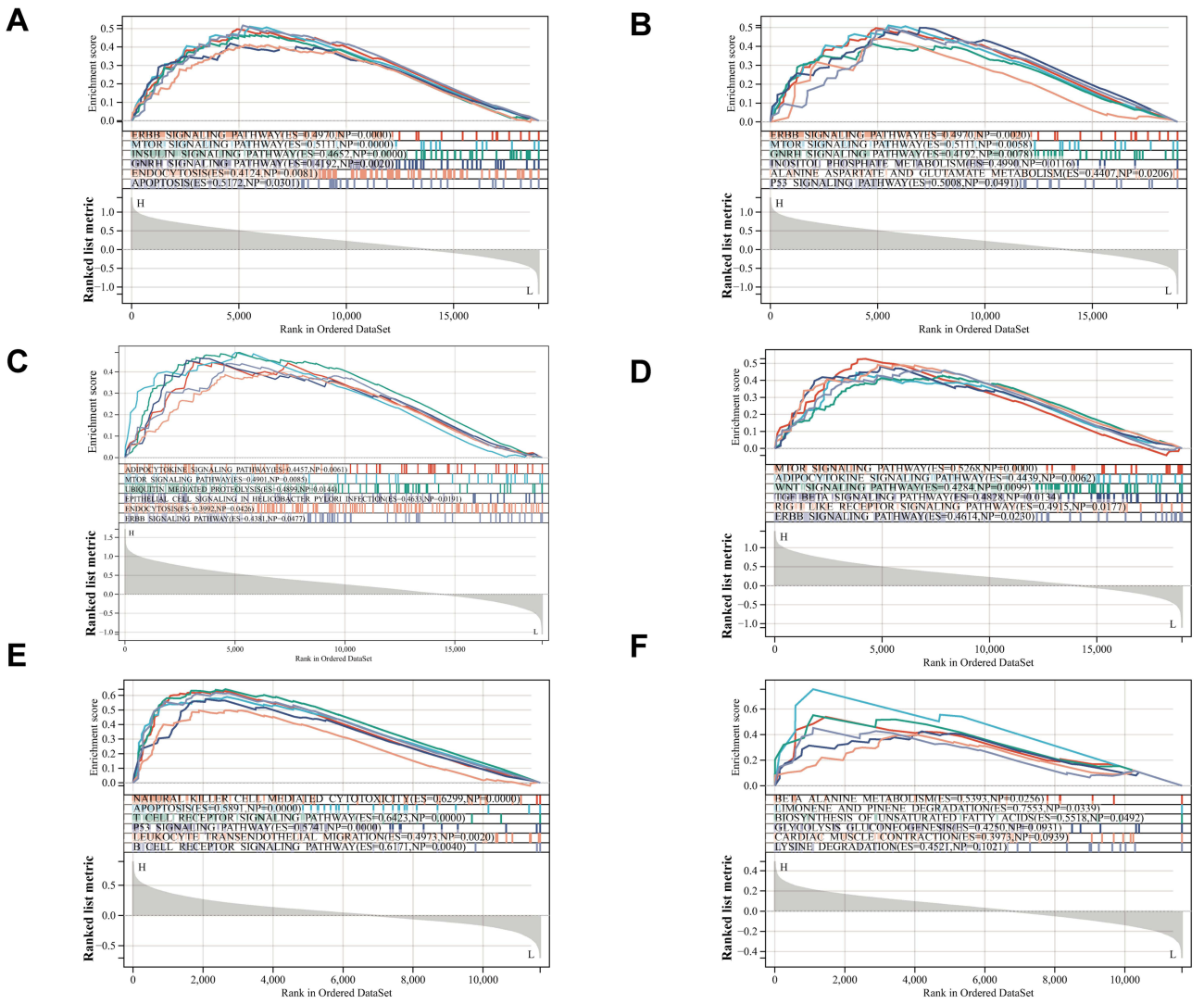

Figure 8 GSEA revealed the enriched pathways of the key genes. (**A**) KPNA3, (**B**) RAB35, (**C**) GLE1, (**D**) RNF139, (**E**) OSMR, and (**F**) PDPK1.

role in CRS-related lipid metabolism. Functional enrichment analysis highlighted key pathways, such as ubiquitin mediated proteolysis, mTOR signaling pathway, neurotrophin signaling pathway and MAPK signaling pathway, associated with inflammation and immune regulation. Immune cell infiltration analysis revealed significant differences in the

Table 1 Top 10 Lipid Metabolism-Related CRS Gene-Targeted Drugs

Term	Adjusted P-value	Odds Ratio	Combined Score	Genes
Fulvestrant MCF7 DOWN	0.11203353762400589	50.766666666666666	333.21384118468507	PDPK1;KPNA3
Estradiol CTD 00005920	0.11203353762400589	18.082429000230892	109.45351111881044	GLE1;RNF139;PDPK1;OSMR;KPNA3
Oxindole i TTD 00009978	0.11203353762400589	285.42857142857144	1542.8675927558304	PDPK1
LY-294002 HL60 UP	0.11203353762400589	190.21904761904761	955.5316921910462	PDPK1
0175029-0000 MCF7 DOWN	0.11203353762400589	12.463973063973064	61.974306797608186	RNF139;RAB35;KPNA3
Bisindolylmaleimide i TTD 00002466	0.11203353762400589	153.6	740.2218192098322	PDPK1
0316684-0000 MCF7 DOWN	0.11203353762400589	147.9037037037037	707.410051609059	OSMR
Paclitaxel CTD 00007144	0.11203353762400589	19.86048879837067	94.6493152532141	PDPK1;OSMR
Microcystin LR CTD 00002422	0.11203353762400589	133.09333333333333	623.0766346487915	PDPK1
Fisetin PC3 DOWN	0.11203353762400589	18.04730983302412	82.76816123537722	RNF139;PDPK1

https://doi.org/10.2147/JIR.S536790

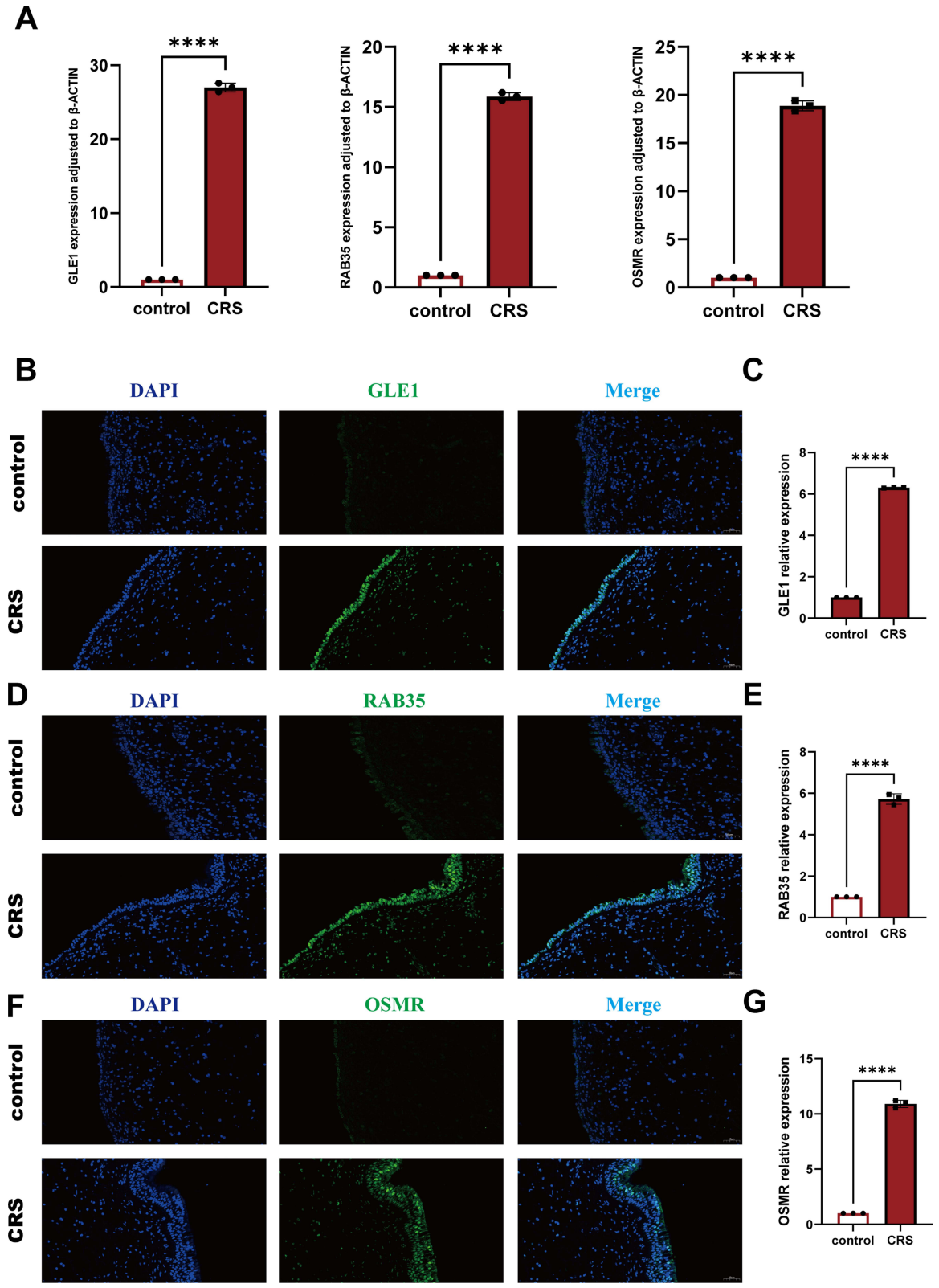

Figure 9 Expression validation of key genes. (**A**) qRT-PCR was used to detect the gene expression levels of GLE1, RAB35 and OSMR. (**B**) Immunofluorescence of GLE1 in epithelial tissues of CRS and control groups (**C**) GLE1 relative expression in immunofluorescence. (**D**) Immunofluorescence of RAB35 in epithelial tissues of CRS and control groups. (**E**) RAB35 relative expression in immunofluorescence. (**F**) Immunofluorescence of OSMR in epithelial tissues of CRS and control groups, and (**G**) OSMR relative expression in immunofluorescence. ****P < 0.0001.

expression of immune cell types, including activated B cells, activated CD8 + T cells, activated dendritic cells, gamma delta T cells, immature B cells, MDSC, macrophages, mast cells, monocytes, natural killer cells, neutrophils, plasmacytoid dendritic cells, regulatory T cells, T follicular helper cells, Type 1 T helper cells, and Type 2 T helper cells. Additionally, a RF+Stepglm[both] model was developed, achieving excellent diagnostic performance (AUC = 0.848), and potential candidate drugs targeting the identified genes were proposed, offering therapeutic possibilities for CRS. Both qRT-PCR and immunofluorescence assays confirmed that the expression of RAB35, GLE1, and OSMR—genes positively associated with CRS in the model—was notably elevated in CRS.

KPNA3 regulates the nuclear import of transcription factors, such as NF-κB, which is essential for inflammation and immune responses. When its expression is inhibited by the active vitamin D metabolite calcitriol, the release of various inflammatory factors is reduced, alleviating asthma symptoms.[16] Additionally, upregulation of KPNA3 expression leads to increased expression of matrix metalloproteinases (MMPs) and cyclooxygenase-2 (COX-2), resulting in cartilage matrix degradation and exacerbated inflammatory responses.[17] These suggest that abnormal KPNA3 expression may play a significant role in the pathogenesis and progression of CRS.

The Rab family proteins, belonging to the small GTPase family, play critical roles in vesicle trafficking, including exosome release, which is essential for cellular communication and immune homeostasis.[18] In asthma, IL-17A, a key pro-inflammatory factor, activates Rab35 through multiple signaling pathways, influencing airway smooth muscle contraction.[19] Conversely, Rab35 knockdown delays TCR downregulation in mouse TH2 cells, leading to increased secretion of cytokines (IL-4, IL-5, and IL-13) and promoting asthma progression.[20] Thus, further investigation is needed to clarify Rab35's role in inflammation.

GLE1 regulates RNA export and stress-response pathways,[21] potentially influencing immune and inflammatory processes. Research by Auttawit Sirichoat et al revealed that GLE1 expression is downregulated during both the infection and clearance stages of *Staphylococcus aureus* in leukocytes.[22] This downregulation may disrupt gene expression and protein synthesis, affecting the host's infection response and recovery. However, the specific molecular mechanisms remain unclear.

RNF139 (TRC8) is an E3 ubiquitin ligase associated with the endoplasmic reticulum (ER) membrane, playing essential roles in protein degradation, lipid metabolism and immune modulation.[23,24] In osteoarthritis (OA), TRC8 accumulation in the ER promotes chondrocyte apoptosis, matrix-degrading enzyme expression, and inflammatory factor release, accelerating disease progression.[25]

Oncostatin M Receptor (OSMR), a cell surface receptor closely linked to IL-31, activates signaling pathways like JAK-STAT and PI3K/AKT, regulating diverse physiological and pathological processes.[26,27] OSMR expression is upregulated in conditions such as atopic dermatitis,[28] Crohn's disease, and ulcerative colitis.[29] In obesity-related inflammation, OSM produced by macrophages binds to OSMRβ on adipocytes, affecting adipocyte function and potentially modulating macrophage polarization states.[30]

3-Phosphoinositide-Dependent Protein Kinase 1 (PDPK1 or PDK1) is a crucial kinase involved in cellular signaling. It maintains CD4 T cell homeostasis and proliferation,[31] promotes microglial polarization to the M2 phenotype to reduce neuroinflammation,[32] and inhibits NLRP3 protein expression, thereby lowering bronchopneumonia-associated inflammation levels.[33]

CRS is a complex inflammatory disease, with lipid metabolism emerging as a significant factor in its pathogenesis. Lipid mediators like prostaglandins (PGs), thromboxane A2 (TxA2), and leukotrienes (LTs) derived from arachidonic acid (AA) play pivotal roles in regulating vascular tone, recruiting immune cells, and promoting inflammatory responses.[34] GSEA data suggest that lipid metabolism might be linked to pathways such as ubiquitin-mediated proteolysis, the mTOR signaling pathway, neurotrophin signaling, and MAPK signaling. Abnormalities in these pathways may affect extracellular matrix remodeling and intracellular signaling, contributing to airway inflammation in asthma and CRS.[35,36] In osteoarthritis (OA), ubiquitin-mediated proteolysis is one of the key pathways enriched with OA-specific DEGs, consistent with our research findings.[37] The mTOR signaling pathway's activation reduces Tregs and impairs their function, causing Th2/Th17 imbalance and persistent inflammation in CRS.[36] Elevated neurotrophin levels in CRS sinus mucosa, such as NGF, neurokinin-1 receptor, and bradykinin-1, indicate its role in polyp formation and inflammation persistence.[38]

Despite regional and racial differences in the inflammatory characteristics of CRS, Th2 inflammation remains a key factor in its pathogenesis and is associated with treatment resistance. Th2 cells and their secreted cytokines play a crucial

role in eosinophil accumulation and immune cell infiltration.[8] Macrophages, derived from bone marrow progenitor cells, are also involved. Specifically, M2 macrophages are associated with eosinophilic CRSwNP inflammation and disease severity, contributing to tissue remodeling. Factors expressed by M2 macrophages, such as TIPE2 and FXIIIA, play important roles in the pathogenesis of CRS.[39] Mast cells are elevated in the epithelium of eosinophilic CRSwNP and participate in inflammation by producing type 2 cytokines. Their activity may be influenced by epithelial-derived cytokines (eg, TSLP, IL-1) and IgE-mediated responses. Mast cells can also enhance the recruitment and cytokine production of ILC2s through the release of PGD2 and LTC4.[40] Our immune cell infiltration analysis revealed significant differences in the expression of macrophages, mast cells, and Type 2 T helper cells between CRS patients and controls, consistent with these findings.

Common CRS treatments include antibiotics, nasal corticosteroids, antihistamines, and decongestants. However, some patients show poor responses due to CRS's complex pathogenesis. Targeted drug development is needed. Using the DSigDB database, we identified promising therapeutic compounds linked to lipid metabolism-associated CRS pathogenic genes. Raloxifene regulates immune and inflammatory responses by antagonizing IL-6 signaling and has shown efficacy in severe COVID-19-associated ARDS.[41] Hesperidin, a flavonoid from citrus fruits, enhances epithelial barrier integrity,[42] modulates T cell subsets, and suppresses inflammation via NF-κB inhibition.[43] Future clinical trials are needed to evaluate the efficacy of these drugs in CRS and develop tailored therapeutic strategies.

Overall, this article highlights the significant role of lipid metabolism in CRS pathogenesis, emphasizing diagnostic model development, targeted treatment, and integrative approaches to understanding complex diseases. In the future, this diagnostic model is expected to achieve early and accurate diagnosis of CRS by detecting the expression characteristics of lipid metabolism related genes in patients; Meanwhile, targeted therapy strategies developed based on key gene targets can guide clinical doctors in developing personalized treatment plans for patients. However, the limitations of this study include the small sample size of the control group, which may affect statistical efficacy, and the lack of functional experimental validation of therapeutic targets, which will be addressed in future research.

Conclusion

Through bulk RNA sequencing and bioinformatics analysis, we identified six key genes associated with lipid metabolism and CRS, and further investigated their involved biological processes and pathways, confirming the significant impact of lipid metabolism on the immune microenvironment and its crucial role in CRS progression. Additionally, leveraging a comprehensive machine learning framework, we constructed a genetic diagnostic model for lipid - metabolism - related CRS, aiming to screen patients who are suitable for lipid metabolism - targeted therapy. The limitations of this study include the small sample size and the need for functional validation of the proposed treatment objectives.

Abbreviations

CRS, Chronic rhinosinusitis; DEGs, differentially expressed genes; WGCNA, weighted correlation network analysis; PPI, Protein–protein interaction; GSEA, gene set enrichment analysis; GO, Gene Ontology; KEGG, Kyoto Encyclopedia of Genes and Genomes; MDSCs, myeloid-derived suppressor cells; STRING, Search Tool for the Retrieval of Interacting Genes/Proteins; AUC, area under the curve.

Data Sharing Statement

The datasets supporting the conclusions of this article are included within the article (and its additional file(s)).The bulk-RNA sequencing data during the current study can be obtained from GSA (Genome Sequence Archive) PRJNA1205537 (https://www.ncbi.nlm.nih.gov/bioproject/PRJNA1205537).

Ethics Approval and Consent to Participate

This study was approved by the Ethics Committee of the First Affiliated Hospital of Chongqing Medical University and conducted in accordance with the guidelines of the Helsinki Declaration of the World Medical Association (No.2022-K301).

Author Contributions

All authors made a significant contribution to the work reported, whether that is in the conception, study design, execution, acquisition of data, analysis and interpretation, or in all these areas; took part in drafting, revising or critically reviewing the article; gave final approval of the version to be published; have agreed on the journal to which the article has been submitted; and agree to be accountable for all aspects of the work.

Funding

National Natural Science Foundation of China, Grant/Award Number: 81970864 and 8247113; Natural Science Foundation of Chongqing, Grant/Award Number: CSTB2024NSCQ-MSX0642; Foundation of State Key Laboratory of Ultrasound in Medicine and Engineering, Grant/Award Number: 2023KFKT001).

Disclosure

The authors report no conflicts of interest in this work.

References

1. Bachert C, Marple B, J SR, et al. Adult chronic rhinosinusitis. *Nat Rev Disease Primers*. 2020;6(1):86. doi:10.1038/s41572-020-00218-1
2. Liang Y, Xie R, Xiong X, et al. Alterations of nasal microbiome in eosinophilic chronic rhinosinusitis. *J Allergy Clin Immunol*. 2023;151(5):1286–1295.e2. doi:10.1016/j.jaci.2022.11.031
3. Halderman A, Lane AP. Genetic and immune dysregulation in chronic rhinosinusitis. *Otolaryngol Clin North Am*. 2017;50(1):13–28. doi:10.1016/j.otc.2016.08.009
4. Karadeniz EB, Aliyeva C, Aydemir S, et al. Chronic rhinosinusitis in patients with primary immunodeficiency. *Int Arch Allergy Immunol*. 2023;184(3):302–310. doi:10.1159/000527265
5. Yan B, Lan F, Li J, Wang C, Zhang L. The mucosal concept in chronic rhinosinusitis: focus on the epithelial barrier. *J Allergy Clin Immunol*. 2024;153(5):1206–1214. doi:10.1016/j.jaci.2024.01.015
6. Kim B, Rothenberg ME, Sun X, et al. Neuroimmune interplay during type 2 inflammation: symptoms, mechanisms, and therapeutic targets in atopic diseases. *J Allergy Clin Immunol*. 2024;153(4):879–893. doi:10.1016/j.jaci.2023.08.017
7. Poddighe D, Vangelista L. Staphylococcus aureus Infection and persistence in chronic rhinosinusitis: focus on leukocidin ED. *Toxins*. 2020;12(11):678. doi:10.3390/toxins12110678
8. Ryu G, Kim DW. Th2 inflammatory responses in the development of nasal polyps and chronic rhinosinusitis. *Curr Opin Allergy Clin Immunol*. 2020;20(1):1–8. doi:10.1097/ACI.0000000000000588
9. W VT, Armstrong M, M KJ, et al. Altered tissue specialized pro-resolving mediators in chronic rhinosinusitis[J]. *Prostaglandins, Leukotrienes Essent Fatty Acids*. 2021;164:102218. doi:10.1016/j.plefa.2020.102218
10. Beegun I, S KD, Alusi G, et al. Dysregulated maresin concentrations in plasma and nasal secretions from patients with chronic rhinosinusitis. *Front Immunol*. 2021;12:733019. doi:10.3389/fimmu.2021.733019
11. Robinson PZ, Frank DN, Ramakrishnan VR. Inflammation resolution and specialized pro-resolving lipid mediators in chronic rhinosinusitis. *Exp Rev Clin Immunol*. 2023;19(8):969–979. doi:10.1080/1744666X.2023.2232554
12. Żelechowska P, Brzezińska-Błaszczyk E, Wiktorska M, et al. Adipocytokines leptin and adiponectin function as mast cell activity modulators. *Immunology*. 2019;158(1):3–18. doi:10.1111/imm.13090
13. Yang B, Gu M, Hong C, et al. Integrated machine learning and bioinformatic analysis of mitochondrial-related signature in chronic rhinosinusitis with nasal polyps. *World Allergy Organ J*. 2024;17(10):100964. doi:10.1016/j.waojou.2024.100964
14. Shu F, Wang Y, Li L, et al. Multi-omics integration and machine learning identify and validate neutrophil extracellular trap-associated gene signatures in chronic rhinosinusitis with nasal polyps. *Clin Immunol*. 2025;275:110473. doi:10.1016/j.clim.2025.110473
15. Fokkens WJ, Lund VJ, Hopkins C, et al. European position paper on rhinosinusitis and nasal polyps 2020. *Rhinology*. 2020;58(Suppl S29):1–464. doi:10.4193/Rhin20.401
16. Agrawal T, Gupta GK, Agrawal DK. Calcitriol decreases expression of importin α3 and attenuates RelA translocation in human bronchial smooth muscle cells. *J Clin Immunol*. 2012;32(5):1093–1103. doi:10.1007/s10875-012-9696-x
17. Yin X, Wang JQ, Yan SY. Reduced miR-26a and miR-26b expression contributes to the pathogenesis of osteoarthritis via the promotion of p65 translocation[J]. *Mol Med Rep*. 2017;15(2):551–558. doi:10.3892/mmr.2016.6035
18. Lin P, Chu M, Liu Y, et al. Revealing potential rab proteins participate in regulation of secretory autophagy machinery. *Kaohsiung J Med Sci*. 2024;40(7):642–649. doi:10.1002/kjm2.12848
19. Bulek K, Chen X, Parron V, et al. IL-17A recruits Rab35 to IL-17R to mediate PKCα-dependent stress fiber formation and airway smooth muscle contractility. *J Immunol*. 2019;202(5):1540–1548. doi:10.4049/jimmunol.1801025
20. W YC, D HC, Zhou M, et al. Regulation of T cell receptor signaling by DENND1B in T H 2 cells and allergic disease. *Cell*. 2016;164(1–2):141–155. doi:10.1016/j.cell.2015.11.052
21. Qiu X. Screening of differential proteins binding to Nox1 promoter in TNF-α-induced A549 cells and preliminary functional study of CSRP2. *Master's thesis*, Southern Medical University, 2013,http://www.cnki.net
22. Sirichoat A, Kaewseekhao B, Nithichanon A, et al. Proteomic profiles and protein network analysis of primary human leukocytes revealed possible clearance biomarkers for staphylococcus aureus infection. *Current Microbiol*. 2023;80(10):335. doi:10.1007/s00284-023-03450-6
23. P LJ, Brauweiler A, Rudolph M, et al. The TRC8 ubiquitin ligase is sterol regulated and interacts with lipid and protein biosynthetic pathways. *Mol Cancer Res*. 2010;8(1):93–106. doi:10.1158/1541-7786.MCR-08-0491

24. Jiang W, Song BL. Ubiquitin ligases in cholesterol metabolism. *Diabet Metabol J*. 2014;38(3):171. doi:10.4093/dmj.2014.38.3.171
25. Li K, Yang P, Zhang Y, et al. DEPTOR prevents osteoarthritis development via interplay with TRC8 to reduce endoplasmic reticulum stress in chondrocytes. *J Bone Miner Res*. 2020;36(2):400–411. doi:10.1002/jbmr.4176
26. Chattopadhyay S, Tracy E, Liang P, et al. Interleukin-31 and oncostatin-M mediate distinct signaling reactions and response patterns in lung epithelial cells. *J Biol Chem*. 2007;282(5):3014–3026. doi:10.1074/jbc.M609655200
27. Cornelissen C, Lüscher-Firzlaff J, M BJ, et al. Signaling by IL-31 and functional consequences. *Eur J Cell Biol*. 2012;91(6–7):552–566. doi:10.1016/j.ejcb.2011.07.006
28. Boniface K, Diveu C, Morel F, et al. Oncostatin M secreted by skin infiltrating T lymphocytes is a potent keratinocyte activator involved in skin inflammation. *J Immunol*. 2007;178(7):4615–4622. doi:10.4049/jimmunol.178.7.4615
29. Kokkotis G, Filidou E, Tarapatzi G, et al. Oncostatin M induces a pro-inflammatory phenotype in intestinal subepithelial myofibroblasts. *Inflammatory Bowel Dis*. 2024;30(11):2162–2173. doi:10.1093/ibd/izae098
30. Sanchez-Infantes D, Stephens JM. Adipocyte oncostatin receptor regulates adipose tissue homeostasis and inflammation. *Front Immunol*. 2021;11:612013. doi:10.3389/fimmu.2020.612013
31. Sun F, X WF, Zhu H, et al. SUMOylation of PDPK1 is required to maintain glycolysis-dependent CD4 T-cell homeostasis. *Cell Death Dis*. 2022;13 (2):181. doi:10.1038/s41419-022-04622-1
32. Wei Y, Chen J, E CG, et al. Rosmarinic acid regulates microglial M1/M2 polarization via the PDPK1/akt/HIF pathway under conditions of neuroinflammation. *Inflammation*. 2021;44(1):129–147. doi:10.1007/s10753-020-01314-w
33. Yang M, Li L. Remimazolam attenuates inflammation in bronchopneumonia through the inhibition of NLRP3 activity by PDPK1 ubiquitination. *Chem Biol Drug Des*. 2024;103(1):e14438. doi:10.1111/cbdd.14438
34. Zhang C, Wang K, Yang L, et al. Lipid metabolism in inflammation-related diseases. *Analyst*. 2018;143(19):4526–4536. doi:10.1039/C8AN01046C
35. P GL, G GP, L SJ, et al. Characteristic DNA methylation profiles in peripheral blood monocytes are associated with inflammatory phenotypes of asthma. *Epigenetics*. 2014;9(9):1302–1316. doi:10.4161/epi.33066
36. Chang L, Wu H, Huang W, et al. IL-21 induces pyroptosis of treg cells via akt–mTOR–NLRP3–caspase 1 axis in eosinophilic chronic rhinosinusitis. *J Allergy Clin Immunol*. 2023;152(3):641–655.e14. doi:10.1016/j.jaci.2023.04.013
37. Ge Y, Chen Z, Fu Y, et al. Identification and validation of hub genes of synovial tissue for patients with osteoarthritis and rheumatoid arthritis. *Hereditas*. 2021;158(1):37. doi:10.1186/s41065-021-00201-0
38. Konstantinou GN, Koulias C, Koulias C, et al. Further understanding of neuro-immune interactions in allergy: implications in pathophysiology and role in disease progression. *JAsthma Allergy*. 2022;15:1273–1291. doi:10.2147/JAA.S282039
39. Kong IG, Kim DW. Pathogenesis of recalcitrant chronic rhinosinusitis: the emerging role of innate immune cells. *Immun Net*. 2018;18(2):e6. doi:10.4110/in.2018.18.e6
40. Kato A. Immunopathology of chronic rhinosinusitis. *Allergol Int*. 2015;64(2):121–130. doi:10.1016/j.alit.2014.12.006
41. Hong S, Chang J, Jeong K, et al. Raloxifene as a treatment option for viral infections. *J Microbiol*. 2021;59(2):124–131. doi:10.1007/s12275-021-0617-7
42. Park H, Yu J. Hesperidin enhances intestinal barrier function in Caco-2 cell monolayers via AMPK-mediated tight junction-related proteins. *FEBS Open Bio*. 2023;13(3):532–544. doi:10.1002/2211-5463.13564
43. Salama A, O GMS, N YN, et al. Immunoregulatory role of hesperidin against ovalbumin (OVA)-induced bronchial asthma and depression in rats. *Naunyn-Schmiedeberg's Arch Pharmacol*. 2024;397(5):3363–3378. doi:10.1007/s00210-023-02833-7